Surface Properties of LiCoO2 Investigated by XPS Analyses and Theoretical Calculations

ARTICLE *in* THE JOURNAL OF PHYSICAL CHEMISTRY C · APRIL 2009

Impact Factor: 4.77 · DOI: 10.1021/jp803266w

Surface Properties of $LiCoO_2$ Investigated by XPS Analyses and Theoretical Calculations

L. Dahéron,[†] H. Martinez,*[,†] R. Dedryvère,[†] I. Baraille,[†] M. Ménétrier,[‡] C. Denage,[‡] C. Delmas,[‡] and D. Gonbeau[†]

IPREM, UMR 5254, Université de Pau, Hélioparc Pau Pyrénées, 64053 Pau cedex 9, France, and ICMCB CNRS, Université Bordeaux I, 87 av. du Dr A. Schweitzer, 33608 Pessac cedex, France

Received: April 15, 2008; Revised Manuscript Received: February 3, 2009

XPS analyses (core peaks and valence spectra), under highly controlled conditions, have been carried out on stoichiometric $LiCoO_2$ and lithium-overstoichiometric $Li_{1+y}Co_{1-y}O_{2-y}$ ($y \sim 0.05$) materials, with significant changes observed in the oxygen peaks. Indeed, beside the component attributed to the O^{2-} anions of the crystalline network, a second one with variable intensity has been observed on the high binding energy side. With the support of ab initio biperiodical calculations on $LiCoO_2$, we propose that this peculiar oxygen signature is partially associated, for $LiCoO_2$, to undercoordinated oxygen atoms coming from (0 0 1) oriented surfaces. These surface oxygen anions are significantly less negative than the ones of the lattice. These results, in conjunction with SEM analyses for the lithium overstoichiometric material (as prepared and thermally treated), show that the presence of defects (oxygen vacancies) has to also be considered in the overstoichiometric case. As in battery material, all reactions (the intercalation but also the parasitic ones) occur through the surface; characterization of its crystallographic nature (as well as its electronic properties) is a key point to a better understanding and optimization of Li ion batteries.

1. Introduction

$LiCoO_2$ is the most widely used positive electrode material for commercial Li-ion batteries, and its bulk properties have been extensively studied.[1−6] When this material is synthesized at high temperature, it exhibits the ideal layered α-$NaFeO_2$-type structure ($R\bar{3}m$ space group) with an ABCABC stacking of oxygen layers, the Li and Co ions ordering in alternate (1 1 1) planes of the cubic close-packed oxygen lattice.[7] The lithium ions can be deintercalated from $LiCoO_2$ with a very good reversibility and a high electrochemical potential, giving rise to batteries with good cyclability (up to 4.2 V vs Li^+/Li) and high voltage.[1,8]

Electrochemical characteristics of lithium-ion batteries using $LiCoO_2$ as a positive electrode are strongly dependent on the synthesis conditions of the material, and particularly on the nominal Li/Co ratio. Several studies have been devoted to the effect of nonstoichiometry in $LiCoO_2$,[9−11] with the excess lithium being reported to affect the capacity and the cycle life of Li-ion batteries, as the capacity decreases and the capacity fade increases with increasing nominal Li/Co ratio. Li-overstoichiometry in $LiCoO_2$ was first mentioned in 1997 by Carewska et al.,[12] who considered the presence of some Co^{2+} ions. In 2003, Levasseur et al. [13] excluded the presence of Co^{2+} ions in lithium-overstoichiometric material and proposed a structural model, taking into account several experimental observations (^{7}Li NMR, magnetic data, chemical analyses, etc.). According to these authors, the excess Li replaces some cobalt ions in the CoO_6 slabs, and the charge deficit associated with a Li ion in a Co site is compensated for by an O^{2-} vacancy. This leads to a formula $[Li]_{interslab}[Co^{III}_{1-3t}Co^{3+(IS)}_{2t}Li_t]_{slab}[O_{2-t}]$, involving an intermediate spin configuration (IS) for 2*t* Co ions in a square-based pyramidal site.

The performances of Li-ion batteries are also closely linked to phenomena occurring at the surfaces of the electrodes, and there is strong evidence that most of lithiated transition metal oxides are reactive with electrolyte solutions.[14,15] Then, the knowledge of surface pecularities of such materials, especially $LiCoO_2$, is a first step to understand their surface chemistry. Surprisingly and in contrast to the numerous reports and high precision achieved in the bulk analyses of the positive electrode materials, less attention has been devoted to the surface properties of such materials.

Therefore, this study presents XPS investigations under highly controlled conditions achieved on Li-stoichiometric $LiCoO_2$ and lithium-overstoichiometric $Li(Li_xCo_{1-x})O_{2-x}$ materials for a better understanding of their surfaces. Our results are discussed with respect to biperiodical ab initio calculations. Even if several papers report theoretical calculations on transition metal oxide surfaces like TiO_2 (anatase or rutile),[16,17] this study is to our knowledge the first one concerning surface modeling of $LiCoO_2$.

2. Experimental and Computational Details

2.1. Materials Synthesis. Stoichiometric $LiCoO_2$ was prepared by direct solid-state reaction from Li_2CO_3 (Alfa Aesar, min. 99%) and Co_3O_4 (calcination at 400 °C for 12 h under O_2 of $CoCO_3$ (Alfa Aesar, min. 99%)) with a starting Li/Co ratio of 1.0. The finely ground mixture was pressed into pellets and heated in a gold crucible at 600 °C for 12 h under O_2 flow, then crushed and reheated at 900 °C under O_2 for 15 days.

The lithium-overstoichiometric material was prepared by direct solid-state reaction from Li_2CO_3 (Alfa Aesar, min. 99%) and Co_3O_4 (calcination at 400 °C for 12 h under O_2 of $CoCO_3$ (Alfa Aesar, min. 99%)) with a starting Li/Co ratio of 1.2. The finely ground mixture was pressed into pellets and heated in a gold crucible at 600 °C for 15 h under O_2 flow, then crushed and reheated at 800 °C for 1 h under O_2. The reaction product was finely crushed and washed by deionized water. After filtration and drying, the intermediate product was mixed with

* Corresponding author. E-mail herve.martinez@univ-pau.fr.
[†] IPREM.
[‡] ICMCB CNRS.

10.1021/jp803266w CCC: $40.75
Published on Web 03/16/2009

Li_2CO_3 (Alfa Aesar, min. 99%) with a mass ratio of 1.0, then pressed into pellets and heated in a gold crucible at 900 °C for 24 h under O_2 flow. The resulting mixture was carefully washed with deionized water and dried at 100 °C in air.

The stoichiometry of both compounds was checked by ^{7}Li MAS NMR according to previous results obtained by Levasseur et al.[13] (see Supporting Information, section 1). Both compounds were crushed into powders for XPS analyses.

2.2. XPS Measurements. XPS measurements were carried out with a Kratos Axis Ultra spectrometer using a focused monochromatized Al Kα radiation ($h\nu = 1486.6$ eV). For the Ag $3d_{5/2}$ line, the full width at half-maximum (fwhm) was 0.58 eV under the recording conditions. The analyzed area of the samples was (300 × 700) μm^2. Peaks were recorded with a constant pass energy of 20 eV. The pressure in the analysis chamber was ca. 5×10^{-7} Pa. To prevent the samples from moisture/air exposure on the analysis site, the XPS spectrometer was directly connected through a transfer chamber to a nitrogen dry box. Short acquisition time control spectra were recorded at the beginning and at the end of each experiment to check the nondegradation of the samples. The binding energy scale was calibrated from the carbon contamination using the C 1s peak at 285.0 eV. Core peaks were analyzed using a nonlinear Shirley-type background.[18] The peak positions and areas were optimized by a weighted least-squares fitting method using 70% Gaussian, 30% Lorentzian line shapes. Quantification was performed on the basis of Scofield's relative sensitivity factors.[19]

2.3. Computational Details. All calculations were performed using the periodic ab initio CRYSTAL03 code.[20] The crystalline orbitals are expanded in terms of localized atomic Gaussian basis set, in a way close to the LCAO (linear combination of atomic orbitals) method commonly adopted for molecules. Different functionals as hybrid B3LYP (based on Becke's three parameters adiabatic connection exchange functional[21] in combination with Lee−Yang−Parr's correlation functional[22]) and PWGGA (developed on the Perdew−Wang functionals[23−26] for both exchange and correlation potentials) have been tested in this work. Some controversy exists concerning both functionals giving accurate physical values (band gaps, magnetic moments, etc.).[27−29] In this work, PWGGA and B3LYP approaches give similar results, at the level of surface geometries (relaxation phenomena) and Mulliken-type charge analysis. Concerning the band gap, the B3LYP hybrid functional overestimates it in comparison to the experimental value. In this paper, the discussion of theoretical results is presented using the PWGGA functional, which could be considered a classical approach for DFT calculations achieved on solids, as the B3LYP functional is commonly used for the description of the ground-state energetics of small molecules. The comparison between both approaches is reported in the Supporting Information (section 2).

In order to decrease further the computational cost of these calculations, the Hay−Wadt large core[30] and Durand and Barthelat effective core pseudopotentials[31] were used to model the core electrons of cobalt and oxygen atoms. Lithium atoms were treated at an all-electron level. The standard valence basis sets (1−1 G + 4−1 G for cobalt, 4−1 G for oxygen, and 6−1 G for lithium; Table 1) already optimized in an earlier study[32] were used for orbital expansion when solving the DFT-SCF equation iteratively. The number of k points in the first irreducible Brillouin zone (Pack-Monkorst lattice[33]) at which the Hamiltonian matrix is diagonalized are equal to 20 and 32 for, respectively, the slabs and the bulk.

TABLE 1: Exponents (bohr^{-2}) and Contraction Coefficients of the (Individually Normalized) Gaussian Functions Adopted for Lithium (All Electron), Cobalt (Hay-Wadt Large Core Pseudopotential) and Oxygen (Durand and Barthelat Effective Core Pseudopotential)[a]

		coefficients	
shell type	exponents	s	p,d
Li (1s)	8.400 [+2]	2.640 [−3]	
	2.175 [+2]	8.500 [−3]	
	7.230 [+1]	3.350 [−2]	
	1.966 [+1]	1.824 [−1]	
	5.044 [+0]	6.379 [−1]	
	1.500 [+0]	1.000 [+0]	
Li (2sp)	5.140 [−1]	1.000 [+0]	1.000 [+0]
Co (4sp)	6.500 [−1]	1.000 [+0]	1.000 [+0]
Co (5sp)	2.200 [−1]	1.000 [+0]	1.000 [+0]
Co (3d)	4.371 [+1]		2.950 [−2]
	1.189 [+1]		1.649 [−1]
	4.003 [+0]		4.032 [−1]
	1.397 [+0]		4.695 [−1]
Co (4d)	4.467 [−1]		1.000 [+0]
O (2sp)	2.371 [+1]	1.694 [−2]	2.638 [−2]
	6.227 [+1]	−1.615 [−1]	1.151 [−1]
	2.108 [+0]	1.124 [−1]	2.990 [−1]
	7.065 [−1]	6.700 [−1]	4.709 [−1]
O (3sp)	2.245 [−1]	1.000 [+0]	1.000 [+0]

[a] From ref 32. $y[\pm z]$ stands for $y \times 10^{\pm z}$.

TABLE 2: Optimized Lattice Constants of $LiCoO_2$ Compared to Experimental Values[7]

	exp	LCAO - PWGGA
a_{hex} (Å)	2.815	2.826
c_{hex} (Å)	14.050	14.088
z_{ox} (Å)	0.260	0.258

In the following text, " slabs " represents a finite number of atomic layers. When only the last atoms from the outer surface plane are concerned, we used the term "extreme surface".

In optimizing the geometry, we allowed the relaxation of all atoms. A modified conjugated gradient algorithm[34] has been implemented in the CRYSTAL03 code to optimize the fractionnary atomic coordinates. Moreover, in the present work, the optimization code (PENTE)[35] developed in our laboratory and interfaced with the CRYSTAL03 code allows one to carry out numerical optimization of any other parameter—cell parameters or basis set exponents—(Newton−Raphson method). In geometry optimization, the criterion for convergence on the total energy is set to 10^{-8} Hartree.

$LiCoO_2$ (high temperature form) crystallizes in the trigonal system ($R\bar{3}m$ space group) with the α-$NaFeO_2$-type structure. This structure, named O3, can be represented as an ordered rock salt type with an ABCABC stacking of oxygen planes, with the Li^+ and Co^{3+} ions ordered in alternate layers of octahedral sites of the (1 1 1) planes. The conventional hexagonal cell used for space group $R\bar{3}m$ will be adopted in this study, the (1 1 1) cubic plane becoming (0 0 1). In this configuration, the structure of $LiCoO_2$ is characterized by the lattice constants a_{hex} and c_{hex}, representing, respectively, the Co−Co intra and interlayer (c_{hex}/3) distances, and by z_{ox}, representing the position of oxygen atom along theh c_{hex} axis. Cobalt, lithium, and oxygen occupy the Wyckoff crystallographic positions 3*a* (0,0,0), 3*b* (0,0,0.5), and 6*c* (0,0,z_{ox}), respectively. The computed lattice constants, obtained by minimizing the total energy, are reported and compared to experimental values in Table 2.

As the main subject of this paper is the knowledge of the $LiCoO_2$ surface, 2D calculations were also carried out. The

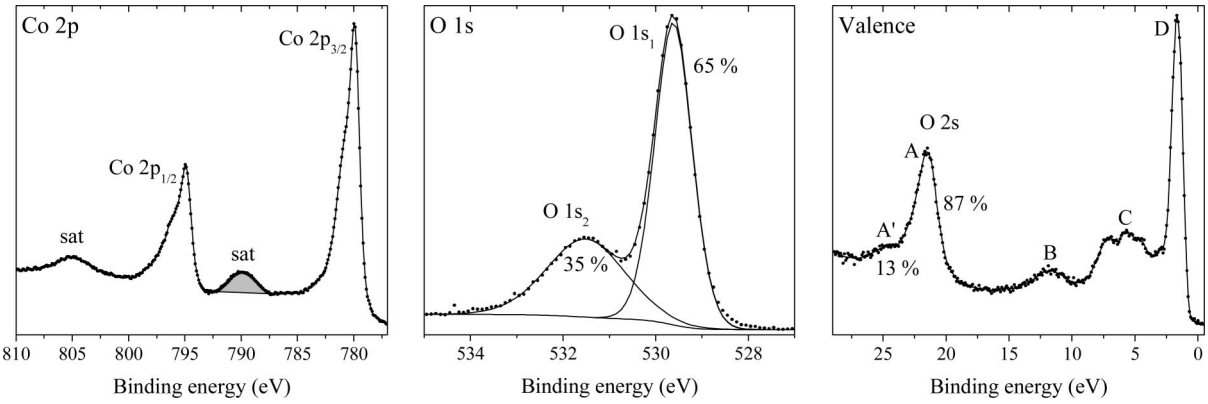

Figure 1. Co 2p and O 1s core peaks and the valence band of $LiCoO_2$.

theoretical details adopted to model the different surfaces are presented in section 3.2.2.

3. Results and Discussion

3.1. XPS Analysis of $LiCoO_2$. Although $LiCoO_2$ was the subject of thorough XPS analyses in a previous study,[36] it seems important to recall here the principal characteristics of this material.

Figure 1 displays the Co 2p and O 1s core peaks and the valence spectrum of $LiCoO_2$.

3.1.1. Cobalt 2p. Considering the spin−orbit coupling, the spectrum is split in two components ($2p_{3/2}$ and $2p_{1/2}$), with an intensity ratio of about 2/1. Each component presents a main line (780 and 795 eV) and a satellite peak (790 and 805 eV). The presence of the satellite peak can be interpreted, at the simplest level of approximation, by a molecular orbital description.[37−39] In the ground state, the electronic configuration of $LiCoO_2$ can be written as $2p^6\ 3d^6\ L$: six electrons in the Co 3d-shell and a filled ligand shell L (oxygen 2p-shell). Photoexcitation on the Co site may lead to several final states after the creation of the 2p core hole. The main line is mainly characterized by the $2p^5\ 3d^7\ L^{-1}$ configuration, where one electron is transferred from the ligand shell L to the metal 3d-shell (screening effect). The satellite can be assigned to $2p^5\ 3d^6\ L$ and $2p^5\ 3d^8\ L^{-2}$ configurations. This effect is known as ligand-to-metal charge transfer ("shakeup"), with the position and the intensity of this shakeup satellite being strongly dependent on the oxidation state and the environment of the metal.

3.1.2. Oxygen 1s. The O 1s spectrum of $LiCoO_2$ exhibits two typical peaks (O $1s_1$ and O $1s_2$). The narrow peak O $1s_1$ at 529.7 eV (relative atomic percentage: 65%) is characteristic of oxygen atoms of the crystalline network. The larger peak with low-intensity O $1s_2$ at higher binding energies (531.6 eV, relative atomic percentage: 35%) may be assigned to weakly adsorbed species at the surface. This sole hypothesis is however unlikely: First, considering the drastic experimental conditions used, we observed a very low carbon contamination percentage (12%) compared with the usual percentage of any surface, which is at about 25%. Note that C1s XPS core peak presents four components; the main one (9%), located at 285 eV, is assigned to hydrocarbon contamination and to carbon atoms bound only to C or H atoms. The three other components (assigned to carbon atoms in a one-, 286.5 eV, two-, 288.5 eV, and three-oxygen environment, 289.5 eV) represent 3%. Then, the percentage of carbon atoms with an oxygen environment is low and could not be the sole cause of the $O1s_2$ component located at high binding energy, which accounts for 16% absolute atomic percentage. Second, we have recently studied the acid−base properties of the $LiCoO_2$ surface, by adsorption of gaseous base and acid (NH_3 and SO_2), which is the subject of a forthcoming paper. The acidic surface reacts with the incoming base to form an acid−base pair, which can be identified in XPS. Indeed, measurement of the binding energy (BE) associated to nitrogen (N 1s) leads to the determination of the adsorption type and the resulting species. The reaction of NH_3 with Brönsted acid sites (OH groups) involves the formation of ammonium ion, and the corresponding BE for N 1s is about 401−402 eV. Our XPS results concerning the acidity of $LiCoO_2$ show that the surface acidic sites are all Lewis-type (N 1s core peak located at about 399.4 eV [46]) and the presence of a hydroxyl group (Brönsted acid sites) is excluded (no N 1s core peak at about 401, 402 eV [46]). The corresponding N 1s XPS core peak is added in the Supporting Information (section 3). Consequently, the O 1s component located at high binding energy could be associated to the so-called "unusual" oxygen atoms from the extreme surface, a behavior commonly observed but not precisely assigned for several metal oxides.[40] This assumption will be discussed in light of theoretical calculations performed on $LiCoO_2$.

3.1.3. Valence Spectrum. The valence spectrum of $LiCoO_2$ presents four main bands labeled A, B, C, and D, which require band structure calculations for a definite attribution. However, the narrow band at lower binding energies (D: 1.7 eV) and the one on the high binding energy side (A: 21.5 eV) could be mainly assigned respectively to t_{2g} orbitals of Co 3d states and O 2s states. Assignment of the B band at 12 eV and the C triplet structure with maxima located at 4.4, 5.7, and 7.3 eV, are more precisely discussed in the following section from density of states.

The band mainly associated with O 2s orbitals located at 21.5 eV presents two components (A and A′), as the O 1s core peak. Nevertheless, and by reference to the main A peak, the intensity of the second component A′ (at high binding energy, ca. 25 eV) is weaker (relative atomic percentage: 13%) than the one for the O 1s core peak. This can be explained by the analysis depth associated with each XPS signal. Indeed, the kinetic energy of the photoelectrons coming into the analyzer is about 950 eV for O 1s and 1450 eV for O 2s, resulting in a photoelectron escape depth about 1.5 times greater for the valence spectrum than for the O 1s core peak. Consequently, the valence bands are more representative of the bulk, while the core peaks are characteristic of the extreme surface composition. These results strengthen the assumption proposed previously, i.e., the ascription of the second oxygen component (at high binding energy) to oxygen atoms from the extreme surface.

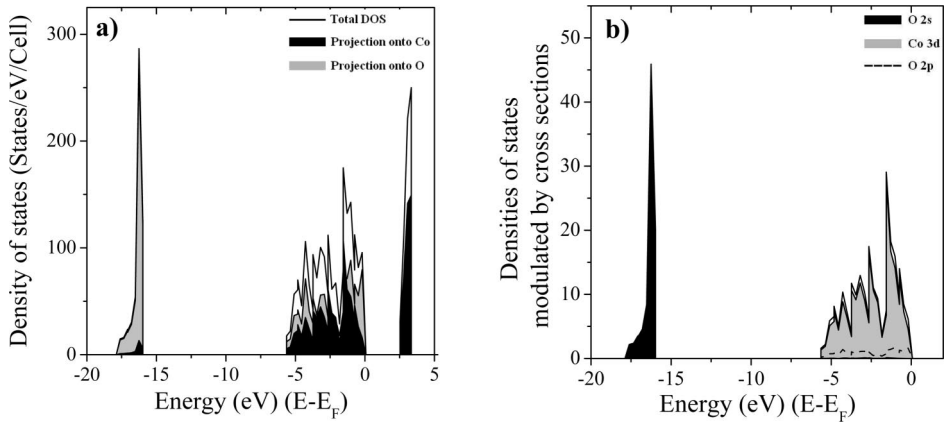

Figure 2. Density of states. (a) Total density of states (full line) and projections onto Co and O states, respectively, represented as black and gray areas (b) Total DOS (occupied states only) modulated by the photoionization cross sections.[19] O 2s, Co 3d, and O 2p modulated states are, respectively, represented as black and gray areas and dashed line.

3.2. Surface Modeling on the Stoichiometric Compound. ***3.2.1. 3D Calculations.*** To improve our knowledge of the $LiCoO_2$ surface, we have performed LCAO-B3LYP and PWGGA calculations. As previously mentioned, we only report PWGGA results, as both functionals give similar results. Bulk properties of $LiCoO_2$ have been the subject of various theoretical calculations.[32,41−43] In the context of modeling different surfaces of $LiCoO_2$, the first step is to consider the bulk material with our own computational details and compare the density of electronic states (DOS) curves to the valence band.

The computed DOS (Figure 2) agrees with previous theoretical calculations.[43] As expected, the main contribution of the O 2s orbital is observed between −17.9 and −16 eV ($E - E_F$). The DOS shape between −5.7 and −1.8 eV is consistent with the structure observed experimentally (Figure 1): this large band mainly results from interactions between Co 3d and O 2p states. The same interactions are observed between −1.8 and 0 eV. Note that the small band labeled B corresponds to a shakeup satellite with a poorly screened 3d hole ($3d^5$ configuration)[44,45] and cannot be predicted by first-principle calculations. Indeed, in calculations within the density functional approach, the electronic correlation in the ground state is accounted for but does not take into account final state effects associated with satellite peaks.

In addition to the DOS curves analysis, note that the calculated band gap is ca. 2.5 eV, which is consistent with the experimental value of 2.7 eV.[46] Note that the band gap is calculated by subtracting the values corresponding to the minimum of the conduction band and the maximum of the valence band.

Figure 2b displays the total density of states modulated by the photoionization cross section (tabulated by Scofield[19]). It confirms the main assignments performed previously and shows that the cobalt d orbitals dominate in the [−1.8 to 0 eV] energy window.

3.2.2. 2D Calculations. We have defined several unit cells that are periodically repeated in two dimensions and built from the optimized lattice parameters of the bulk as a starting point ($a = 2.826$ Å and $c = 14.088$ Å). Three kinds of surfaces were considered in our calculations: (0 0 1), (1 1 0), and (1 0 0). These surfaces were modeled by considering slabs that consist of a finite number of atomic layers. The relaxation of the surface is taken into account by optimizing the cell parameters and all the atomic positions in order to obtain the equilibrium geometry.

The results obtained for the (1 0 0) slab (which can be visualized in the Supporting Information, section 4) lead to a complete surface reorganization during geometrical optimization and to high surface energy. This reconstruction involves large (yet still in the atomic scale) displacements of the surface atoms. This phenomenon usually occurs with the less stable surfaces. Therefore, the main presence of such planes at the surface of crystallites appears unlikely during the synthesis process.

In this way, we only report the results obtained with the two other types of surfaces (0 0 1) and (1 1 0), which, respectively, correspond to the plane of stacking and the densest plane (at an atomic level) of $LiCoO_2$.

3.2.3. The $LiCoO_2$ (0 0 1) Surface. Our slab model consists of four monatomic layers (the stoichiometry requires a multiple of four-layer slab) where the outer layers consist of oxygen and Li atoms. As Figure 3a displays, the sequence of stacking up is the following: O - Co - O - Li - O - Co - O - Li. Obviously, only the surface with oxygen atoms at the top should be considered. Moreover, we have checked that the number of layers is sufficient to effectively describe the electronic properties of $LiCoO_2$ (compared to the bulk) and allow a reasonable computing time (CPU), as the inversion is the only symmetry operator of this model. Starting from bulk values for geometrical parameters, Table 3 presents the main results of the optimization: it displays first the vertical coordinates of the first four atomic planes (interlayer relaxation) as an essential part of the relaxation phenomena occurring at the surface, and second the main bond length changes of the planes considered compared to the bulk.

Even if the relaxation is a small and subtle rearrangement of the surface layers, it is nevertheless significant energetically, as the difference between the unrelaxed and relaxed slab is about 3.51 eV. It involves adjustments in the layer spacing perpendicular to the surface: the first layer of atoms is typically slightly moved toward the second layer (i.e., d [L1 − L2] < d bulk = d unrelaxed slab by 0.16 Å), and this contraction of the first two layer distance is compensated by an increase of d [L2 − L3]. Obviously, the bond lengths follow the same trends, as the distance between O_{L1} (i.e., oxygen atom from first layer) and Co_{L2} (i.e., cobalt atom from second layer) decreases and $Co_{L2} - O_{L3}$ increases (compared to the unrelaxed slab). Note that the third and fourth layers display a contraction, which explains the decrease of the lithium−oxygen distance. On the whole, these results are consistent with a classical relaxation phenomenon involving rearrangements of extreme surface (and near surface) atoms, with this process being driven by the energy of the system, i.e., the desire to reduce the surface free energy.

3.2.4. The $LiCoO_2$ (1 1 0) Surface. As each layer exhibits the $LiCoO_2$ stoechiometry, the only parameter of interest is the

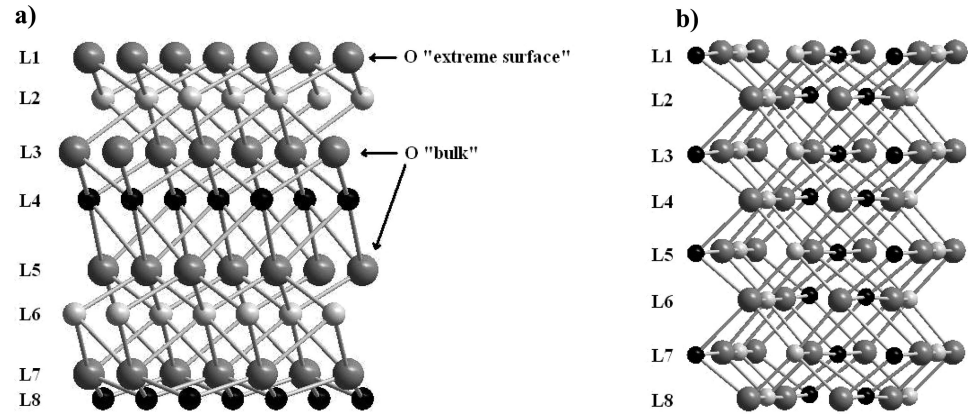

Figure 3. Schematic view of the surfaces studied. The Li atoms are denoted as black circles, and Co and O as small light and large dark gray circles, respectively. (a) (0 0 1) surface (8-monolayer model). (b) (1 1 0) surface (8-monolayer model).

TABLE 3: Geometric Parameters of Unrelaxed and Relaxed (0 0 1) Slabs of $LiCoO_2$[a]

distances (Å)	unrelaxed slab (bulk values)	relaxed slab
d [L1 − L2]	1.050	0.890
d [L2 − L3]	1.050	1.159
d [L3 − L4]	1.295	1.042
d [L4 − L5]	1.295	1.535
d [L5 − L6]	1.050	0.993
d [O_{L1} − Co_{L2}]	1.940	1.885
d [Co_{L2} − O_{L3}]	1.940	2.026
d [O_{L3} − Li_{L4}]	2.090	1.962
E (eV)	−3838.38	−3841.89

[a] d [Lx − Ly] represents the interlayer distance between xth and yth layers; d [A_{Lx} − B_{Ly}] stands for atomic distance between A and B atoms, belonging to xth and yth layers, respectively.

number of layers that gives a suitable representation of the surface with a reasonable computing time (no symmetry operator except inversion). As previously, we chose to study an eight-layer slab (Figure 3b), and optimization results are presented in Table 4. For a nonexhaustive presentation, only the results corresponding to the first four atomic planes are presented. The spacing between these planes exhibits the same trends as those noticed previously for the (0 0 1) surface: d [L1 − L2] and d [L3 − L4] decrease by, respectively, 0.146 and 0.064 Å, and d [L2 − L3] increases by 0.099 Å. Note that the main contraction of the first two atomic planes has the same magnitude for both slabs, but the interlayer distance is larger for the (1 1 0) slab than for the (0 0 1) one. Thus, the relaxation phenomenon is less significant for the (1 1 0) surface, in relation to its highest density of atoms per layer.

For this surface, two types of bonds ought to be examined: bonds within the same plane and those between planes, as all atoms (O, Co, Li) are contained in the same layer. All interatomic distances from the same layer exhibit a contraction compared to the unrelaxed slab. The interatomic distances between layers d [A_{Lx} − B_{Ly}] change in the same way as the layer spacing, a contraction for [A_{L1} − B_{L2}] and [A_{L3} − B_{L4}] (with a weaker amplitude for the third and the fourth layers) and an enlargement for [A_{L2} − B_{L3}] (more significant for lithium−oxygen bonds).

3.2.5. Surface Energies. Even if a real comparison of the surface energies of the (001) and (110) surface is difficult as kinetic aspects (which occur during the synthesis of the real active material of Li-ion batteries studied in this paper) are not taken into account in the theoretical approach, the following results may contribute to a better fundamental knowledge of the $LiCoO_2$ surface.

TABLE 4: Geometric Parameters of Unrelaxed and Relaxed (1 1 0) Slabs of $LiCoO_2$[a]

distances (Å)	unrelaxed slab (bulk values)	relaxed slab
d [L1 − L2]	1.413	1.267
d [L2 − L3]	1.413	1.512
d [L3 − L4]	1.413	1.349
d [Li− -O_{L1}]	2.090	1.990
d [Li_{L2} − O_{L2}]	2.090	1.977
d [Li_{L3} − O_{L3}]	2.090	1.959
d [Li_{L4} − O_{L4}]	2.090	1.966
d [Co_{L1} − O_{L1}]	1.940	1.831
d [Co_{L2} − O_{L2}]	1.940	1.918
d [Co_{L3} − O_{L3}]	1.940	1.925
d [Co_{L4} − O_{L4}]	1.940	1.926
d [Li_{L1} − O_{L2}]	2.090	2.028
d [Co_{L1} − O_{L2}]	1.940	1.899
d [O_{L1} − Li_{L2}]	2.090	2.002
d [O_{L1} − Co_{L2}]	1.940	1.902
d [Li_{L2} − O_{L3}]	2.090	2.188
d [Co_{L2} − O_{L3}]	1.940	2.020
d [O_{L2} − Li_{L3}]	2.090	2.225
d [O_{L2} − Co_{L3}]	1.940	1.992
d [Li_{L3} − O_{L4}]	2.090	2.057
d [Co_{L3} − O_{L4}]	1.940	1.925
d [O_{L3} − Li_{L4}]	2.090	2.063
d [O_{L3} − Co_{L4}]	1.940	1.936
E (eV)	−15 372.56	−15 373.13

[a] d [Lx − Ly] represents the interlayer distance between xth and yth layers; d [A_{Lx} − B_{Ly}] stands for atomic distance between A and B atoms. belonging to xth and yth layers, respectively.

TABLE 5: Surface Energies for the Surface Studied

	E (eV)	n (number of units created per slab or for the bulk)	E(surf) (eV.Å^{-2})
bulk	−1922.59	1	
(0 0 1)	−3841.89	2	0.228
(1 1 0)	−15373.13	8	0.149

Table 5 gives the total energy per $LiCoO_2$ for each surface studied, and the differences with the bulk value to obtain the surface energy. To calculate this value, one has to account for the number of $LiCoO_2$ units created at the surface versus the number of units contained in the 3D unit cell,[47] with the surface energy being defined as the total energy per repeating cell of the slab minus the total energy of the same number of atoms of the perfect crystal, divided by the surface area of the two sides of the slab, i.e.,:

$$E(\text{surf}) = [E(\text{slab}) - nE(\text{bulk})]/2A$$

where E(slab) is the energy of the slab containing $n$$LiCoO_2$ units, E(bulk) is the unit cell bulk energy, and A is the area of the surface unit cell (7.21 Å^2 for (0 0 1), 25.49 Å^2 for (1 1 0)). The most stable surface is relative to the (1 1 0) slab (0.149 eV.Å^{-2}, T0able 5). However, as we consider that the bottom side of the (0 0 1) surface is formed by lithium atoms, it probably overestimates the surface energy, as the both terminations are not identically stable.

Note that the sequence O - Co - O - Li - O - Co - O - Li (eight layers) was adopted to preserve the stoichiometry, which is necessary to present the electronic properties of the sample (band gap and DOS). Considering this fact, we have also achieved calculations using seven, nine (001) layers with the respective following sequence:

7 layers: O - Co - O - Li - O - Co - O

9 layers: Li - O - Co - O - Li - O - Co - O - Li

In this way, we can calculate the surface energy for various slabs (seven and nine layers), among which one ends with oxygen atoms and the other with lithium atoms. The average of both surface energies should be compared with the eight-layer slab, which presents oxygen and lithium for both sides.

In order to calculate these surface energies for nonstoichiometric slabs, we can use the method described by Y. X. Wang et al.[48] We first calculate the cleavage energy for unrelaxed O and Li terminated surfaces. Surfaces with both terminations arise simultaneously under cleavage of the crystal, and the relevant cleavage energy is distributed equally between created surfaces. Therefore, one can assume that the cleavage energy (E_{cle}) is the same for both terminations. This cleavage energy is defined as

$$E_{cle} = 1/4(E_{unrelslab,O} + E_{unrelslab,Li} - 4E_{bulk})$$

where $E_{unrelslab,O}$ and $E_{unrelslab,Li}$ are unrelaxed oxygen (seven layers) and lithium (nine layers) terminated slab energies; E_{bulk} is the energy per $LiCoO_2$ bulk unit cell; the factor of 1/4 comes from the fact that four surfaces upon cleavage procedure are created; the factor 4 comes from the fact that the seven layers and the nine layers together represent four unit cells. The cleavage energy leads to a value of 0.125 98 au (atomic units).

Next, we can calculate the (negative) relaxation energies for each of O and Li terminations, when both sides of slabs relax: $E_{rel,x} = 1/2(E_{relslab,x} - E_{unrelslab,x})$, where $E_{rel,x}$ is the slab energy after relaxation, x = O or Li; $E_{rel,O}$ and $E_{rel,Li}$ have, respectively, the values of (−0.014 12 au) and (−0.245 93 au).

We note that for the surface terminated by lithium atoms, the energy of relaxation is much more negative than for the surface terminated by oxygen atoms. This difference means, as attempts, that the relaxation of the surface terminated by lithium atoms is noticeable and that, to achieve the stability, the surface has to be reconstructed.

Last, the surface energy sought is just a sum of the cleavage and relaxation energies:

$$E_{s,x} = E_{rel,x} + E_{cle}$$

TABLE 6: Atomic Net Charges Resulting from a Mulliken Population Analysis for the Bulk and Both Surfaces Studied

	atom	resulting net charge (PWGGA)
bulk (infinite 3D crystal)	Li	0.996
	Co	1.177
	O	−1.086
(0 0 1) (8 layer slab model)	Li (L4)	0.996
	Co (L2)	1.182
	O "extreme surface" (L1)	−0.308
	O "bulk" (L3)	−1.181
	O "bulk" (L5)	−0.997
(1 1 0) (8 layer slab model)	Li	0.994
	Co	1.076
	O	−1.049

The average surface energy for both terminations is equal to 0.060 967 au (1.659 eV). This value, divided by the area of the two-dimensional (0 0 1) unit cell (7.216 Å^2) leads to a surface energy equal to 0.230 eV. Å^{-2}. It could be compared to the value calculated for the eight-layer slab reported in Table 5 (0.228 eV.Å^{-2}). Both values are very close, which means that our calculation, which preserves the stoichiometry (the eight-layer slab), is not unrealistic in a theoretical point of view.

Note that this kind of calculation for the surface energy could be used for the (1 1 0) surface, where both terminations are identical:

$$E_{cle} = 1/2(E_{unrelslab,(110)} - 8E_{bulk})$$

$$E_{rel(110)} = 1/2(E_{relslab,(110)} - E_{unrelslab,(110)})$$

$E_{s(110)} = E_{rel,(110)} + E_{cle} = 1/2(E_{relslab,(110)} - E_{bulk})$; this expression is identical to that used at the beginning of this section.

In conclusion, the value of $E_{s,(110)}$ is still lower than $E_{s,(001)}$ (7−9 layers or 8 layers), but as we mentioned before, a real comparison with the surface energy of the (1 1 0) surface is difficult in this work. Note that, even if the theoretical surface energetically favored is (1 1 0), (0 0 1) one should be present in $LiCoO_2$ crystallites at the same time, as we will discuss in the following section.

3.2.6. Mulliken Charge Analysis and XPS Results. It is well-established that the binding energies determined by XPS for the core electrons of an atom are dependent on the chemical state of this atom. Generally, as the positive character of an atom increases, so does the binding energy of its core electrons. Different relations between chemical shifts and real charge variations have been used successfully.[49] At the simplest level of approximation, the correlation between binding energy and Mulliken-type charge can be written as follows: $\Delta E = k\Delta q$, where ΔE is the experimental shift of binding energy, Δq is the net charge variation, and k is a constant characteristic of the element. In order to get more insight into XPS results (O 1s core peak) of $LiCoO_2$, we have performed Mulliken charge analysis on these surfaces.[50] Table 6 presents the resulting so-called net charges on Li, Co, and O atoms for each surface studied, and the differences with the bulk values for comparison.

For the (0 0 1) surface, while charges on Li and Co atoms are very close to those for the bulk, two types of oxygen atoms (depending on the plane considered) are evidenced. Indeed,

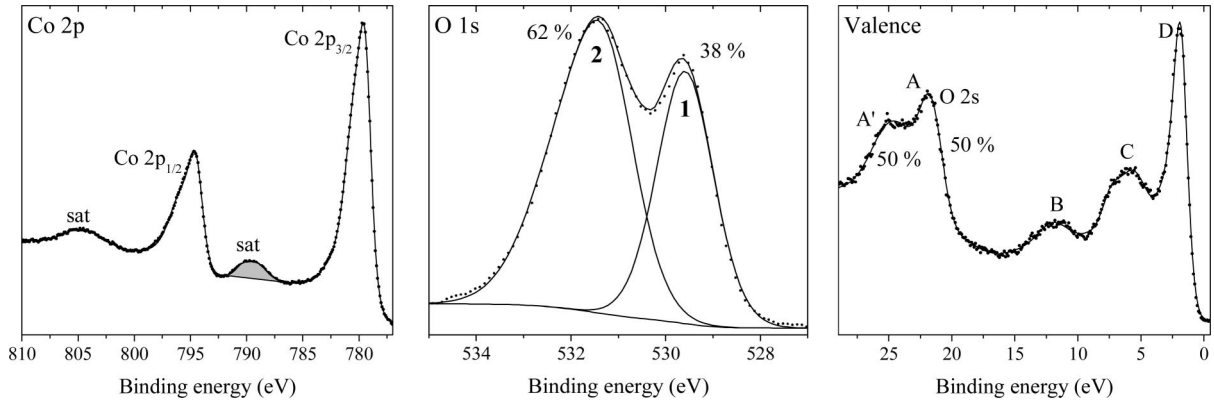

Figure 4. Co 2p and O 1s core peaks and the valence band of lithium-overstoichiometric material.

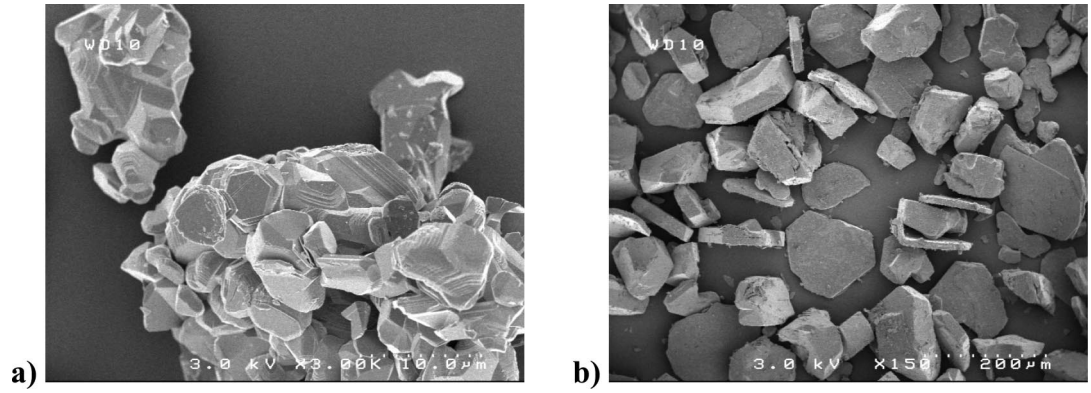

Figure 5. SEM images of $LiCoO_2$ (a) and lithium-overstoichiometric material (b).

oxygen atoms from the outer layer (O "extreme surface") are less charged ($q_{net} = -0.308$ e$^-$) than the ones from the third (or fifth) layer (O "bulk"; average $q_{net} = -1.08$ e$^-$: this value is the average between the q_{net} charge of oxygen atoms from the third and fifth layers), which are quite similar to those in the bulk material ($q_{net} = -1.086$ e$^-$; Table 6). This difference corresponds to a significant reduction of the surface charge for the polar (0 0 1) surface. For the (1 1 0) surface, charges on Li, Co, and O atoms are very close to those for the bulk material. All the oxygen atoms appear equivalent (q_{net}=−1.049 e$^-$) in contrast to the (0 0 1) surface, with the typical deviation of the Mulliken charge for the eight layers being around 5×10^{-2} e$^-$. Note that another sequence of stacking up for the 001 surface (as O - Li - O - Co - O - Li - O - Co) exhibits similar results at the level of Mulliken charge analysis.

Thus, the oxygen atoms from the third (or fifth) atomic layer of (0 0 1) surface and from the (1 1 0) surface present roughly the same net charge and can be assigned to oxygen atoms from the network of $LiCoO_2$, where the corresponding O 1s XPS core peak is located at 529.7 eV. This is consistent with the Mulliken charge analysis for the bulk, which leads to a net charge equal to −1.086 e$^-$, very close to the ones obtained, respectively, for O "bulk" from the (0 0 1) slab and O from the (1 1 0) slab. Furthermore, the second component of the oxygen XPS core peak located toward high binding energies reflects in first approximation the appearance of a more positive charge, and could be thus associated to oxygen atoms coming from (0 0 1) surfaces (O "surf"), with these atoms presenting a net charge less negative than those from the bulk. Let us recall that the XPS results do not explain this component on the sole basis of adsorbed species at the surface. In addition, because of the exponential attenuation of the peak intensities with the photoelectron escape depth z ($I(z) = I_0 \exp[(-z)/(\lambda_i \cos \theta)]$, λ_i = inelastic electron mean free path, θ = angle of emission with respect to the surface normal), the contribution of those O "surf" is not negligible and can be evaluated (with $\lambda_i \approx 1.16$ nm[51]) at about 16% of the total O 1s peak intensity.

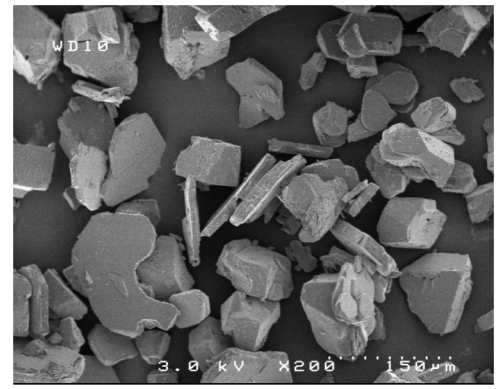

Figure 6. SEM image of stoichiometric (ex-overstoichiometric) $LiCoO_2$.

3.3. Lithium-Overstoichiometric $Li(Li_xCo_{1-x})O_{2-x}$ Material. The above results, based on XPS investigations and theoretical calculations, contribute to a better knowledge of surface peculiarities of $LiCoO_2$. As nonstoichiometry has an influence on electrochemical performances of lithium-ion batteries, it seems important to investigate surface peculiarities of such a material.

As mentioned in the Introduction, Li-overstoichiometry in $LiCoO_2$ was first mentioned in 1997 by Carewska et al.,[12] who

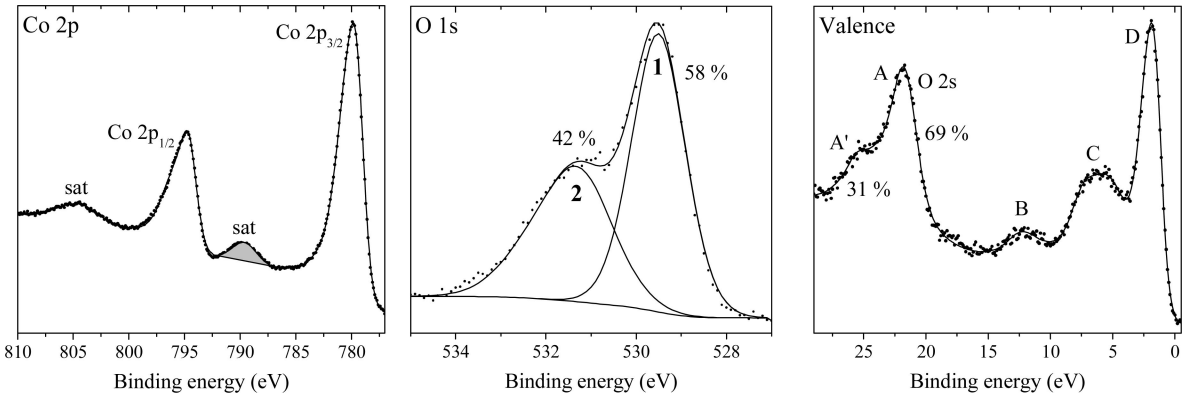

Figure 7. Co 2p and O 1s core peaks and the valence band of stoichiometric (exoverstoichiometric) $LiCoO_2$.

concluded, in a detailed ^6Li and ^7Li NMR study, the possible presence of an unidentified impurity phase and that a small amount of excess Li ions can occupy some sites in the structure, with some of them being interstitial in the vicinity of Co^{2+}. Moreover, they observed a decreasing average cobalt oxidation state with an increasing nominal Li/Co ratio. In 1998, Peeters et al.[52] carried out a very detailed study of nonstoichiometry in $LiCoO_2$. Using ^7Li and ^{59}Co NMR, they have evidenced the existence of paramagnetic Co species, but their actual nature remained unclear. Few years later, Gorshkov et al.[53] and Karelina et al.[54] hypothesized the existence of defects associated with Co^{2+} and strong oxygen deficiency. In 2003, Menetrier et al.[13] suggested that such a defect had a different NMR signature from that present in Li-overstoichiometric samples. Furthermore, they highlighted the fact that the paramagnetic cobalt species in the Li-overstoichiometric compound are very stable in strongly oxidizing conditions, concluding that they are trivalent cobalt ions, rather than divalent ones associated to oxygen vacancies. The local environment of some cobalt ions is however modified by the presence of an oxygen vacancy in the triangular lattice that compensates for the charge of the excess Li occupying Co sites. As a result, the two neighboring cobalt ions adjacent to the oxygen vacancy are in square-based pyramids instead of octahedra, and this local environment change can induce a shift of the relative energies of the 3d orbitals. Therefore, they proposed in this study that the trivalent cobalt ions adjacent to oxygen vacancies adopt an intermediate spin state. Considering the intermediate-spin $Co^{3+(IS)}$, and the low-spin Co^{3+} denoted as Co^{III}, the structural model of the lithium-overstoichiometric material can be written $[Li]_{interslab}[Co^{III}_{1-3t}Co^{3+(IS)}_{2t}Li_t]_{slab}[O_{2-t}]$, in which each O vacancy is surrounded by two $Co^{3+(IS)}$ ions, one Li^+ ion in the CoO_6 slab, and three Li^+ ions in the interslab space.

With theoretical calculations of such a material being difficult to implement, we have only taken XPS results as the basis for our discussion on surface peculiarities of the lithium-overstoichiometric compound.

Figure 4 shows the Co 2p and O 1s core peaks and the valence spectrum of the lithium-overstoichiometric sample.

3.3.1. Cobalt 2p. The Co 2p spectrum of the lithium-overstoichiometric material shows an overall shape similar to that of $LiCoO_2$. It is well-known that the binding energy and the relative area of the satellite peak are a more efficient tool to access the oxidation state of cobalt than the binding energy of the main peak itself. Although Co^{3+} and Co^{2+} in (octahedral) oxygen environment have very close main peak positions (780.0 and 780.3 eV, respectively), the corresponding satellite peaks are very different. Their binding energies are, respectively, located at 790 and 786 eV for Co^{3+} and Co^{2+}[55] and their relative areas are 9% (Co^{3+}) and 33% (Co^{2+}). For the $Li_{1+y}Co_{1-y}O_{2-y}$ compound, the main peak is located at 780 eV and the shakeup satellite accounts for 6.6% of the whole Co $2p_{3/2}$ signal. Thus, Co^{2+} ions are not detected by XPS, in agreement with the nature of the defect assumed by Menetrier et al.[13] The decrease of the shakeup satellite's contribution to the signal compared to $LiCoO_2$ can be explained by a change in either the electronic structure or the environment of some of the cobalt ions.

3.3.2. Oxygen 1s. Compared with $LiCoO_2$, a very different shape is observed for the O 1s core peak of the lithium-overstoichiometric compound. Indeed, beside the O $1s_1$ peak at about 529.7 eV, we note a significant enhancement of the O $1s_2$ component at the high binding energy side. The relative atomic percentages are, respectively, 38% for O $1s_1$ and 62% for O $1s_2$.

Note that, as for the stoichiometry compound, a rather low amount of carbon in oxygen environment (about 7%) was observed, which does not allow an explanation of the O$1s_2$ component (33% absolute atomic percentage). Furthermore, the presence of hydroxyl groups (Brönsted acid sites) after ammonia adsorption was never identified.

3.3.3. Valence Spectrum. As for the stoichiometric sample, four main bands are observed for the overstoichiometric $LiCoO_2$. One can note some differences in the relative intensities of B, C, and D bands, but the most striking change concerns the band at about 25 eV, attributed to O 2s orbitals and broken down into two components A and A′. As compared to the O 1s peak, one can note a decrease of the A′ component intensity (related to contribution of oxygen atoms from the extreme surface). However, the intensity of this component is much larger than for the $LiCoO_2$ compound (Figures 1 and 4).

The whole set of results obtained for O 1s and O 2s peaks in the case of $Li_{1+y}Co_{1-y}O_{2-y}$ compound deserves some comment. Let us recall that the component on the high binding energy side of the O 1s peak has been partially attributed to oxygen atoms coming from (0 0 1) surfaces, the so-called "unusual" oxygen atoms. It is also important to note that the SEM (scanning electron microscopy) analyses of $LiCoO_2$ and $Li_{1+y}Co_{1-y}O_{2-y}$ have revealed significant differences.[56] Indeed, while the SEM image of $LiCoO_2$ presents small crystals with several orientations, the lithium-overstoichiometric sample is mainly formed by large platelets extended in the (001) plane that might preferentially lie perpendicular to their (0 0 1) direction. Therefore, on the extreme surface of a given polycrystalline sample, the number of (0 0 1) type planes will be larger for the $Li(Li_xCo_{1-x})O_{2-x}$ sample than for the $LiCoO_2$ one.

If so, the number of "unusual" oxygen atoms would be larger in the case of the lithium overstoichiometric compound, leading to an enhancement of the oxygen XPS spectrum on the high binding energy side.

In order to expand on this point, additional experiments have been carried out. The lithium-overstoichiometric material was treated for one month under oxygen at 900 °C. By such a treatment, the material gradually transforms to stoichiometric $LiCoO_2$ by losing excess lithium in the form of Li_2O.[13] Like the others, the stoichiometry of the sample was carefully controlled by ^{7}Li NMR (see Supporting Information). It is to be noted that the thermal treatment preserves the morphology of the starting material, i.e., large platelets (0 0 1) oriented as shown by SEM analyses (see Figures 5 and 6), while rendering it stoichiometric. This compound is referred to in the following as stoichiometric (ex-overstoichiometric) $LiCoO_2$. Figure 7 presents the XPS Co 2p and O 1s core peaks and the valence spectrum of the relevant material.

The Co 2p spectrum of the stoichiometric (ex-overstoichiometric) compound shows an overall shape similar to that of the stoichiometric and of the lithium-overstoichiometric ones. Analysis of the O 1s peak reveals that the component at the high binding energy side has an intermediate value between that of $LiCoO_2$ and $Li_{1+y}Co_{1-y}O_{2-y}$ compounds (Figures 1, 4, 7). The same trend is observed when considering the valence spectrum and the A and A′ components of the O 2s peaks (Figures 1, 4, 7).

These XPS results on the stoichiometric (ex-overstoichiometric) $LiCoO_2$ allow us to clarify some points: Compared to $Li_{1+y}Co_{1-y}O_{2-y}$ (with similar particle morphology), the lower intensity of the high binding energy side component shows that Li-overstoichiometry influences the oxygen peak. A reasonable assumption is that the presence of oxygen vacancies in the lithium-overstoichiometric material influences the oxygen atoms surrounding the defects (third neighbors), leading to the creation of under-coordinated oxygen atoms nearby the defects with an XPS signature similar to that of extreme surface oxygen atoms, thus corresponding to some "internal surface effect". Compared to $LiCoO_2$, the enhancement of the high binding energy side component is consistent with a higher proportion of "unusual" oxygen atoms due to possible (0 0 1) orientation of the large platelets. However, this enhancement is a little high, and the presence of defects remaining in the subsurface probably also has to be considered.

4. Conclusion

Our aim in this work was to provide new information on the surface properties of $LiCoO_2$ by means of XPS analysis in combination with biperiodical ab initio calculations. A careful XPS analysis of oxygen peaks (O 1s and O 2s) led us to consider the existence of oxygen atoms from the extreme surface significantly different from the ones of the lattice. The calculations carried out on three surface planes (1 0 0), (0 0 1), and (1 1 0) revealed different relaxation phenomena, with the least stable surface being the (1 0 0) one. In addition, a detailed Mulliken charge analysis highlighted the specific behavior of the (0 0 1) planes characterized by extreme surface oxygen atoms significantly less negative than the ones of the lattice, while such a differentiation did not appear for the (1 1 0) planes. These results enabled us to partially associate a peculiar XPS oxygen signature to undercoordinated oxygen atoms coming from (0 0 1) oriented surfaces. The parallel XPS study of Li-overstoichiometric $Li_{1+y}Co_{1-y}O_{2-y}$ showed that the presence of structural defects, as previously proposed, had to be considered to interpret the enhanced peculiar oxygen signature.

Altogether, by improving our knowledge of the surface properties of $LiCoO_2$, this study constitutes a first step toward a better understanding of the surface chemistry of such materials, that plays a very important role in the parasitic reactions occurring during electrochemical cycling of $LiCoO_2$: cobalt dissolution, catalytic effect toward electrolyte oxidation. These results clearly show that an optimization of the particle morphology not limited to the particle size, but including the nature of the crystallographic plane at the crystallite surface, can improve the performances of the batteries.

Supporting Information Available: Additional information as described in the text. This material is available free of charge via the Internet at http://pubs.acs.org.

References and Notes

(1) Mizushima, K.; Jones, P. C.; Wiseman, P. J.; Goodenough, J. B. *Mater. Res. Bull.* **1980**, *15*, 783.
(2) Reimers, J. N.; Dahn, J. R. *J. Electrochem. Soc.* **1992**, *139*, 2091.
(3) Ohzuku, T.; Ueda, A. *J. Electrochem. Soc.* **1994**, *141*, 2972.
(4) Amatucci, G. G.; Tarascon, J.-M.; Klein, L. C. *J. Electrochem. Soc.* **1996**, *143*, 1114.
(5) Ménétrier, M.; Saadoune, I.; Levasseur, S.; Delmas, C. *J. Mater. Chem.* **1999**, *9*, 1135.
(6) Alcántara, R.; Lavela, P.; Tirado, J. L.; Zhecheva, E.; Stoyanova, R. *J. Solid State Electrochem.* **1999**, *3*, 121.
(7) Orman, H. J.; Wiseman, P. J. *Acta Crystallogr., Sect. C* **1984**, *40*, 12.
(8) Whittingham, M. S. *Chem. Rev.* **2004**, *104*, 4271.
(9) Liu, R.; Yang, X.; Wu, G.; Jin, W.; Lin, Q. *Extended Abstracts of the 12th International Conference on Solid State Ionics*; Halkidiki, Greece 1999.
(10) Levasseur, S.; Ménétrier, M.; Suard, E.; Delmas, C. *Solid State Ionics* **2000**, *128*, 11.
(11) Imanishi, N.; Fujii, M.; Hirano, A.; Takeda, Y.; Inaba, M.; Ogumi, Z. *Solid State Ionics* **2001**, *140*, 45.
(12) Carewska, M.; Scaccia, S.; Croce, F.; Arumugam, S.; Wang, Y.; Greenbaum, S. *Solid State Ionics* **1997**, *93*, 227.
(13) Levasseur, S.; Ménétrier, M.; Shao-Horn, Y.; Gautier, L.; Audemer, A.; Demazeau, G.; Largeteau, A.; Delmas, C. *Chem. Mater.* **2003**, *15*, 348.
(14) Edström, K.; Gustafsson, T.; Thomas, J. O. *Electrochim. Acta* **2004**, *50*, 397–403.
(15) Aurbach, D. *J. Power Sources* **2003**, *11*−*121*, 497–503.
(16) Reinhardt, P.; Heâ, B. A. *Phys. Rev. B* **1994**, *50*, 12015.
(17) Menetrey, M.; Markovits, A.; Minot, C. *Surf. Sci.* **2003**, *524*, 49.
(18) Shirley, D. A. *Phys. Rev. B* **1972**, *5*, 4709.
(19) Scofield, J. H. *J. Electron Spectrosc. Relat. Phenom.* **1976**, *8*, 129.
(20) Saunders, V. R.; Dovesi, R.; Roetti, C.; Orlando, R.; Zicovich-Wilson, C. M.; Harrison, N. M.; Doll, K.; Civalleri, B.; Bush, I. J.; D'Arco, Ph. ; Llunell, M. CRYSTAL03 User's manual University of Turin, 2007, http://www.crystal.unito.it.
(21) Becke, A. D. *J. Chem. Phys.* **1993**, *98*, 5648.
(22) Lee, C.; Yang, W.; Parr, R. G. *Phys. Rev. B* **1988**, *37*, 785.
(23) Perdew, J. P.; Wang, Y. *Phys. Rev. B* **1981**, *23*, 5048.
(24) Perdew, J. P.; Wang, Y. *Phys. Rev. B* **1986**, *33*, 8800.
(25) Perdew, J. P. *Electronic structure of solids*; Akademie Verlag, Berlin, 1991.
(26) Perdew, J. P.; Wang, Y. *Phys. Rev. B* **1992**, *45*, 13244.
(27) Godby, W; Schluter, M.; Sham, L. J. *Phys. Rev. Lett.* **1983**, *51*, 1884.
(28) Muscat, J.; Wander, A; Harrison, N. M. *Chem. Phys. Lett.* **2001**, *342*, 397.
(29) Feng, X *Phys. Rev. B* **2004**, *69*, 155107.
(30) Hay, P. J.; Wadt, W. R. *J. Chem. Phys.* **1985**, *82*, 270.
(31) Durand, P.; Barthelat, J. C. *Theor. Chem. Acta* **1975**, *38*, 283.
(32) Catti, M. *Phys. Rev. B* **2000**, *61*, 1795.
(33) Monkhorst, H. J.; Pack, J. D. *Phys. Rev. B* **1976**, *13*, 5188.
(34) Schlegel, H. B. *J. Comput. Chem.* **1982**, *3*, 214.
(35) PENTE; Dargelos, A. Laboratoire de Chimie Théorique et de Physico-Chimie Moléculaire; UMR CNRS 5624, 1999.
(36) Dahéron, L.; Dedryvère, R.; Martinez, H.; Ménétrier, M.; Denage, C.; Delmas, C.; Gonbeau, D. *Chem. Mater.* **2008**, *20*, 583–590.
(37) Hüfner, S. *Photoelectron spectroscopy: principles and applications*; Springer-Verlag: Berlin, 1995.
(38) Fadley, C. S. *Electron Spectroscopy: theory, techniques and applications*; Brundle, C. R., Baker, A. D., Eds.; Academic Press: London, 1978..
(39) Hüfner, S. *Adv. Phys.* **1994**, *43*, 183.

(40) Dupin, J. C.; Gonbeau, D.; Vinatier, P.; Levasseur, A. *Phys. Chem. Chem. Phys.* **2000**, *2*, 1319.

(41) Aydinol, M. K.; Kohan, A. F.; Ceder, G.; Cho, K.; Joannopoulos, J. *Phys. Rev. B* **1997**, *56*, 1354.

(42) Wolverton, C.; Zunger, A. *Phys. Rev. B* **1998**, *57*, 2242.

(43) Czyžyk, M. T.; Potze, R.; Sawatzky, G. A. *Phys. Rev. B* **1992**, *46*, 3729.

(44) Shen, Z.-W.; Allen, J. W.; Lindberg, P. A. P.; Dessau, D. S.; Wells, B. O.; Borg, A.; Ellis, W.; Kang, J. S.; Oh, S. J.; Lindau, I.; Spicer, W. E. *Phys. Rev. B* **1990**, *42*, 1817.

(45) Van Elp, J.; Wieland, J. L.; Eskes, H.; Kuiper, P.; Sawatzky, G. A.; de Groot, F. M. F.; Turner, T. S. *Phys. Rev. B* **1991**, *44*, 6090.

(46) Guimon, C; Gervasini, A; Auroux, A *J. Phys. Chem.* **2001**, *105*, 10316.

(47) Beltrán, A.; Sambrano, J. R.; Catalayud, M.; Sensato, F. R.; Andrés, J. *Surf. Sci.* **2001**, *490*, 116.

(48) Wang, Y. X.; Arai, M; *Surf. Sci.* **2007**, *601*, 4092–4096.

(49) Siegbahn, K.; Nordling, C.; Johannson, G.; Hedman, J.; Heden, P. F.; Hanu'in, K.; Gelius, U.; Bergmark, T.; Wenne, L. O.; Baer, Y. *ESCA Applied to Free Molecules*; North Holland: Amsterdam, 1969.

(50) Dartigeas, K; Gonbeau, D; Pfister-Guillouzo, G; Ouvrard, G; Levasseur, A *J. Electron Spectrosc. Relat. Phenom.* **1997**, *83*, 45.

(51) Seah, M. P. *Surf. Interface Anal.* **1986**, *9*, 85.

(52) Peeters, M. P. J.; Van Bommel, M. J.; Neilen-ten Wolde, P. M. C.; Van Hal, H. A. M.; Keur, W. C.; Kentgens, A. P. M. *Solid State Ionics* **1998**, *112*, 41.

(53) Gorshkov, V. S.; Kellerman, D. G.; Karelina, V. V. *Russ. J. Phys. Chem.* **1999**, *73*, 921.

(54) Karelina, V. V.; Kellerman, D. E.; Gorshkov, V. S.; Leonidov, I. A.; Patrakeev, M. V. *Russ. J. Phys. Chem.* **2001**, *75*, 496.

(55) Dedryvère, R.; Laruelle, S.; Grugeon, S.; Poizot, P.; Gonbeau, D.; Tarascon, J.-M. *Chem. Mater.* **2004**, *16*, 1056.

(56) Levasseur, S. Ph. D. thesis, University of Bordeaux 1, France; December 2001.

JP803266W